

Array Tomography Workflow for the Targeted Acquisition of Volume Information using Scanning Electron Microscopy

Tilman Franke¹, Irina Kolotuev²

¹Thermo Fisher ²Universite de Lausanne

Corresponding Author

Irina Kolotuev

irina.kolotueva@unil.ch

Citation

Franke, T., Kolotuev, I. Array Tomography Workflow for the Targeted Acquisition of Volume Information using Scanning Electron Microscopy. *J. Vis. Exp.* (173), e61847, doi:10.3791/61847 (2021).

Date Published

July 15, 2021

DOI

10.3791/61847

URL

jove.com/video/61847

Abstract

Electron microscopy is applied in biology and medicine for imaging of cellular and structural details at nanometer resolution. Historically, Transmission Electron Microscopy (TEM) provided insight into cell ultrastructure, but in the recent decade, the development of modern Scanning Electron Microscopes (SEM) has changed the way of looking inside the cells. Even though the resolution of TEM is superior when protein-level structural details are needed, SEM-resolution is sufficient for the majority of the organelle-level cell biology-related questions. The advancement in technology enabled automatic volume acquisition solutions such as Serial block-face imaging (SBF-SEM) and Focused ion beam SEM (FIB-SEM). Nevertheless, to this day, these methods remain inefficient when the identification and navigation to areas of interest are crucial. Without the means for precise localization of target areas before imaging, operators need to acquire much more data than they need (in SBF-SEM), or, even worse, prepare many grids and image them all (in TEM). We propose the strategy of "lateral screening" using Array Tomography in SEM, which facilitates the localization of areas of interest, followed by automated imaging of the relevant fraction of the total sample volume. Array tomography samples are conserved during imaging, and they can be arranged into section libraries ready for repeated imaging. Several examples are shown in which lateral screening enables us to analyze structural details that are incredibly challenging to access with any other method.

Introduction

Despite the importance of EM-related techniques, the effort required to master them keeps the entire field restricted to a small number of specialists. One significant difficulty is the identification and retrieval of a Region of Interest

(ROI) in the samples preserved for EM. The appearance of the same sample considerably differs when analyzed by optic microscopy and after processing for EM observation. The changes for chemically prepared samples include the

anisotropic sample shrinkage after the dehydration steps (~10% in each dimension) and the loss of fluorescence when using osmium in the fixation and staining protocol (**Figure 1A**). For the ultrathin sectioning, the samples are embedded in epoxy or acrylic resins using different strategies (**Figure 1B**). For successful results of this preparation, the entire sample must be fractionated into pieces that do not exceed 1 mm x 1 mm. To meet standard Transmission Electron Microscopy (TEM) observation conditions' requirements, this tiny portion of the sample is further sectioned to 50-150 nm thick slices. The resulting grayscale images show tissue organization and organelle structure of a minute fraction of the entire sample at greater detail than any other microscopy technique (**Figure 1C**). A typical TEM dataset provides 2D information, theoretically extrapolated to understand the processes naturally occurring in a 3D space in cells and tissues. **Figure 1D** presents the challenge of ultrastructural volumes acquisition: if a cube of side 1,000 μm is sectioned at 50 nm thickness, 20,000 sections will be required to cover the entire volume; for a 500 μm side cube, it will be 10,000 sections. To cover a 50 μm x 50 μm x 50 μm volume, 1,000 sections "only" might be necessary. Obtaining this volume manually is practically impossible and extremely challenging to perform with automation. If, in addition to sample depth, we need to cover the entire surface of such hypothetical cubes, the coverage of 1 μm^2 surface at reasonable resolution becomes a serious logistic issue (**Figure 1E**). While for the extraordinary large-scale projects, such as connectomics approaches, the large number of sections is crucial, for the majority of the "mundane" EM projects, generating more sections required for the observation presents a significant disadvantage.

There are several methods to acquire 3D ultrastructural information: serial sectioning Transmission Electron

Microscopy (TEM), TEM tomography, Array Tomography (AT), Serial Block Face Imaging Scanning Electron Microscopy (SBF-SEM), and Focused Ion Beam Scanning Electron Microscopy (FIB-SEM). Principal differences between these methods are the sectioning strategy and whether the image acquisition is coupled to section generation¹. In serial sectioning TEM, sequential sections are collected on slot grids, TEM images are generated from these sequences and aligned^{2,3,4,5}. In TEM tomography, tilt series from 150-300 nm sections on a grid, and when coupled to serial sectioning, provide a very high resolution, though relatively small volumes^{6,7,8}. The AT approach uses physical sectioning with diverse manual and semi-automatic manners of sections collection on relatively large support, such as glass coverslip, silicon wafers or a special tape. For image acquisition, the support is analyzed in SEM, with diverse image acquisition strategies are available^{9,10,11,12,13,14,15}. For SBF-SEM, physical sectioning is achieved using a mini-microtome with a diamond knife set directly inside the SEM chamber, with the SEM image generated from the surface of the resin block^{16,17,18,19}. For FIB-SEM, ion source removes thin layers of the sample, followed by automatic imaging of the exposed surface by the SEM^{20,21}. TEM-tomography and the AT generate physical sections, which can be re-imaged if necessary, while FSBF-SEM and FIB-SEM eliminate the section after imaging. A recent combination of physical sections imaged by a multi-beam SEM provides a combination of methods that solves the "bottleneck" issue of the speed of image acquisition²². Each of these techniques has revolutionized the way EM data can be obtained and analyzed, and each approach has its practical impacts related to a given research question.

Given the nature of the preparation and the scale of the ultrastructural dimensions, it is not straightforward to predict where a specific target structure is located in the sample block (**Figure 1D,E**). One solution for the ROI localization is recording the images from the entire block at the desired resolution from the beginning. The structures of interest can be in the acquired data volume when away from the microscope. Acquisition time and data handling associated with this strategy are problematic. It is desirable to reduce the amount of recorded data, especially if the ROIs are much smaller than the tissue block, i.e., if the objects of interest are specific types of cells (not whole organs). Different correlative light and electron microscopy techniques (CLEM) can be successful when the fluorescence is preserved and localized before or after preparation within the same sample^{23,24,25,26,27,28,29}. Nevertheless, many cellular structures are recognizable even without fluorescence correlation, only based on the known ultrastructure. For these cases, we believe that lateral screening Array Tomography provides a balance tradeoff between the effort invested in ROI localization and the ultrastructural information quality. Using this strategy, a sub-set of sections on the wafer are screened within regular intervals, which can be established based on the ROI's size and nature. Once ROIs are found, data acquisition is set up in a continuous series of sections starting before and ending after the anchor section, collecting the relevant information in a targeted manner.

We present protocols for AT that simplify and accelerate the acquisition of regions or events of interest in numerous sections and yield better-aligned image volumes. Lateral screening and multistep acquisition produce data with very high resolution in precisely targeted regions. The procedure we describe addresses several challenges of 3D EM data acquisition, as it provides for: compatibility with a broad range

of specimens without fundamentally changing the sample preparation workflow; targeted localization for sectioning and SEM acquisitions; reduced time and effort during setup; imaging of regions in multiple sections with better alignment of the resulting volumes; and a smooth stitching and alignment procedure to compile different images into a stitched mosaic picture. We chose to demonstrate the strength of our method with several samples from published and ongoing projects. We believe that this approach can significantly facilitate the generation and acquisition of targeted EM data, even for investigators with limited EM experience.

Protocol

NOTE: Sample preparation methods are described elsewhere^{14,30,31}, and are not covered in this publication. In short, the examples shown were chemically fixed with glutaraldehyde, post-fixed with 1% OsO₄, then treated with 1% aqueous uranyl acetate before embedding in the embed resin. Alternatively, samples can be prepared using high-pressure freezing, freeze substituted with 0.1% uranyl acetate in acetone, and embedded in acrylic resin. Sample blocks were prepared using a flat embedding method that permits a clear view of the sample, facilitating its orientation for the sectioning (**Figure 1B**).

1. Array generation procedure

1. Embedded sample orientation and trimming
 1. Using the binocular/microscope, identify and mark the ROI on the embedded block surface by lightly scratching the block's surface with a razor blade. This will help to orient the sample inside the ultramicrotome and will reduce the sectioning surface.

2. Clamp the sample on the ultramicrotome holder (**Figure 2A**).
 3. Trim the resin around the sample, first with the razor blade (rough trimming) and continue with the diamond trimming tool (fine trimming; **Figure 2A**). Use knives with 20° or 90° edge inclination to ensure that the top and bottom surfaces of the block are parallel to the knife's cutting edge.
NOTE: This step is critical for serial sectioning and acquisition of straight ribbons.
 4. Mix xylene and glue in 3:1 proportion. With an eyelash attached to a toothpick, apply this mixture to the top and the bottom edges of the trimmed block. Let it dry thoroughly.
2. Prepare the array mounting support A (i.e., silicon wafers).
 1. Cut the wafer piece using a wafer cleaving tool (EMS), adjusting its size to the project goal. 2 cm x 4 cm is convenient for both light and electron microscopy observations.
 2. Clean the wafer in distilled water to get rid of the debris.
 3. Glow discharge/plasma clean the surface using standard equipment. The precise parameters will depend on the machine used. Start with the parameters for the grids discharge and empirically adjust the time. This step is crucial for a good spread of the sections on the support while sections are drying and should not be omitted.
 3. Prepare the arrays mounting support B (i.e., glass coverslip)

1. If planning multiplex immuno-labeling experiments, transfer the samples on a coverslip to better detect the fluorescence signal. To improve coverslip adhesiveness, use a detailed gelatin-coating procedure is described previously⁹.
2. Increase the conductivity by coating the slides with the indium-tin-oxide (ITO) or gold by evaporation. Keep the prepared coverslips in a clean environment. Glow discharge the samples as described in 1.2.3.

2. Sectioning of the sample

1. AT knife preparation

NOTE: To generate the arrays, use a modified knife (ATS), designed to facilitate the acquisition of long ribbons. Histo-Jumbo knives or similar knives conceived for the generation of the sections on large supports can serve for AT sectioning as well.

1. Attach the needle to the bottom of the knife using the foamy sticky tape and pierce it (**Figure 2B**). Place the ATS knife in the ultramicrotome holder at 0°. Adjust the edge of the knife parallel to the block surface using the standard procedure.
2. Bring the trimmed block to the edge of the knife in a position ready for sectioning.
3. Place the wafer/coverslip inside the knife basin and fill it with water to the same level as the knife edge. Let the diamond edge of the knife humidify properly and, if necessary, withdraw water using the attached syringe (**Figure 2C**).

2. Array sectioning and transfer

1. Set the microtome to the desired cutting parameters. With the ATS knife, the range of 50-100 nm and a cutting speed of 0.6-1 mm/s are advisable. Start sectioning (**Figure 2Di**).
2. Obtain a ribbon of the length that will cover a targeted z-volume and stop the collection. Depending on the block size, homogeneity of the tissue, and type of resin, the ribbon will be relatively straight (**Figure 2D-ii**). Many samples will not produce straight ribbons, despite the invested effort and the type of knife is used.
3. Depending on the final goal, make one long or several short ribbons aligned side by side. A 2 cm x 4 cm support can conveniently hold 100 to 1,000 sections. The arrangement of the ribbon on the support step is a step that requires dexterity and steady hands. However, the learning curve for this skill is rapidly acquired.
4. Detach the ribbon from the knife-edge using a clean, non-sticky tip of an eyelash glued on the toothpick (**Figure 2Diii**).
5. Using the eyelash, gently move the ribbon above the center of the support medium. At this point, use chloroform or heating pen for stretching of the sections if needed. However, remember that this manipulation may induce ribbon breaking and deformation.
6. Start draining the water by pulling the syringe. For more delicate ribbons or a slower water retraction, let water drip by detaching the syringe from the hose. When the water level is lowering to the wafer level, control the ribbon and reposition it if necessary, by gently pushing the ribbon to the center. After settling

the ribbons on the wafer surface, continue draining until the remaining water is completely retracted from the basin.

NOTE: If not using the bottom water retraction ATS knife, carefully reduce the water from the sides of the ATS knife to not induce turbulence.

7. Leave the sections on the support inside the bath to let dry completely. Depending on the hydrophobicity of the support and environmental humidity level, water will evaporate at a different rate (**Figure 2Div**). It is important to let the sample dry slowly to diminish or altogether avoid all folds on the sample.
 8. Transfer the dry sample to a tightly closed box to protect from dirt contamination and place it to a 60 °C oven for at least 30 min. If required, counterstain sections using heavy metals to enhance the overall contrast.
 9. At the end of the procedure, cautiously clean the knife following the manufacturer's instructions
- NOTE:** The transfer of multiple or serial sections on a wafer (**Figure 2E**) compared to the transfer on a slot grid (**Figure 2F**) change the EM preparation experience entirely. The uninterrupted sectioning and collection of the sections on single support reduces the amount of sectioning and section collection related mistakes frequent in serial sectioning. The equivalent of 100 sections of 1000 μm x 500 μm collected on one wafer corresponds to 33 slot grids (**Figure 2G**).

3. Sample observation

NOTE: This section describes the workflow steps as implemented using a commercially available software (see **Table of Materials**). Any image acquisition software on

any SEM equipped with the correct detectors can be used, however, the specific user actions will differ and will often be more manual.

1. Acquire an overview map of SEM images that reveals section locations on the wafer. A built-in optical camera image helps with defining an SEM image mosaic that covers a ribbon of sections or all sections. Create the mosaic by click-drag with the mouse right on the camera image of the sample and start the **Automatic Acquisition**.

NOTE: Very coarse imaging settings, i.e., 1-2 μm pixel size and 1 μs dwell time suffice. This process is illustrated in **Supplementary Material** (pages 2-7).

2. Locate sections with the **Section Finder Auto Detection** function or locate them manually. Section positions and outlines are retrieved automatically with this software based on image matching. For illustration of this process, see **Supplementary Material** (pages 8 - 15).

3. In case the overview images do not show ROIs clearly, acquire higher resolution images of sections. Use the **Section Preview** function to create and acquire images automatically. This process is illustrated in **Supplementary Material**, pages 16-18. Imaging settings must be chosen according to the nature and size of the ROI that the user searches for.

1. To find optimal settings, activate the **Live Imaging** in the microscope control software and navigate to one ROI. Alter imaging settings until the images show ROIs clearly, but image acquisition is not excessively long.

4. Define imaging regions

NOTE: Several different strategies are proposed.

1. If only a few sections need to be imaged, use the images of sections created so far for navigating to the relevant sections and use the **Zoomable Viewer** that shows all acquired images in their original relative locations to look at all sections. Once a section is found that should be imaged at high resolution, create an imaging region with click-drag. Choose high resolution imaging settings and store the settings in a template. Re-use this template for further sections.
2. To find particularly small or hard to detect rare events, use the Lateral Screening approach. Manually create an imaging region with high resolution imaging settings on every tenth section or on one section per ribbon and acquire the images. Review the images and mark sections that contain the ROI in the software or take a note.
 1. Starting from sections that contain the ROI, navigate forward and backward through the section set and create high resolution imaging regions in the same relative locations for as long as the structure is still visible in the section. This can be done manually or by using the procedure described in the next steps.
3. Acquire images in more than ten consecutive sections. Click **Start Position Refinement** after zooming the image to increase the precision of registered section locations as described in the manual. Doing so decreases the position variability of image series. The procedure is illustrated and explained in **Supplementary Material** pages 19-21.
4. Click-drag on any section to define an imaging region while holding down the **Alt** key and select

Create Tile Set Array from the context menu that opens when the mouse button is released. The software then creates imaging regions in the same relative location in all sections that have been found or marked previously. It is possible to limit imaging to a specific range of sections with the **Section Span** slider.

NOTE: This procedure can be repeated with any number of imaging regions and therefore allows recording many small high-resolution images instead of recording a single larger image on each section.

5. Once created, set up pixel count, pixel size, tiling layout, pixel dwell time, etc. in each image series as needed. Once imaging series are created and set up, they are all listed in a job cue.
5. Configure auto functions and start image acquisition
 1. Create a separate image series for auto functions using the same method as describe in the previous step. Move the image series to a position on the section that contains high-contrast structures.
 2. Set the image series to 1024 x 884 pixels and choose a pixel size corresponding to the highest resolution used in the image series set up in the previous steps. In the list of auto functions, check **Auto Focus** and **Auto Stigmator**.
 3. Select **By Section** in the acquisition sequence controls and make sure the auto functions image is the first item in the list. Start the image acquisition by clicking the **Run** button next to the job cue. These procedures are illustrated in **Supplementary Material**, pages 22-23.

NOTE: It is not necessary to manually pre-focus on each section. During the recording session, whenever the microscope advances to a new section, the auto functions will be executed before all other images are recorded in this section.

4. Data alignment and analysis

1. Data export
 1. Ensure that data is saved in .tif format, so there is no need for a dedicated export function. Sort data into a folder structure that corresponds directly to the layers and elements in the Layer Tree.
 2. Once image mosaics have been recorded, use the **StitchAll** function to automatically stitch all tiles.
2. Stack alignment and cropping in Fiji

NOTE. Many software packages (free and commercial) can be used to work with Array Tomography data. The steps below are shown with open-source program Fiji³² because it is widely available and contains all the required functions.

 1. Import a stack of images (or stitched images) into Fiji as a virtual stack.
 2. If contrast/brightness needs to be normalized, choose **Enhanced Contrast...** from the **Process** menu. Set **Saturated Pixels** to 0.1 or less, and check **Process all Slices**.
 3. From the Plugins menu, choose **Registration | Linear Stack Alignment with SIFT**.
 4. Choose **Rigid** or **Affine** from the **Expected Transformation** drop-down menu. Otherwise, keep the default settings. Start the alignment by clicking **OK**.

NOTE: Loading the data as Virtual Stack allows Fiji to handle stacks of any size. The output of the alignment is created in RAM; however, this can limit the maximum size of stacks that can be processed. In that case, use **Register Virtual Stack Slices**, which is a folder-to-folder implementation of the same registration algorithm. Once registration is complete, load the output data as a virtual stack.

5. Crop the image stack by clicking **Crop** so that it contains only the ROI.
6. Save the stack as a single .tif image or series of .tif images.

NOTE: Critical steps of Array Tomography are shown in **Figure 3**.

Representative Results

The examples below aim to demonstrate the versatility of the recommended workflows. The case study illustrations are projects for which we had difficulty obtaining satisfying results with any other techniques. We chose *Drosophila* adult to illustrate typical challenges one might encounter with numerous types samples. This tubular organ of about 6mm long, 500-1000 μm in cross-section, is divided into different regions with a unique function and cellular composition (**Figure 4A**)³³. Depending on the sectioning orientation, the dimensions of the gut profile and its appearance on the section vary. Either transversely or longitudinal orientated sections are relatively large, and only a couple can be placed on a single TEM grid (**Figure 2F**). Only a small portion of the tissue can be imaged in the FIB, and for the SBF-SEM, the difficulty is similar to any non-homogeneous samples. AT provides an efficient tradeoff for the analysis of such samples and flat embedding facilitates the ROI localization. Careful trimming the excess of resin around the selected area (**Figure 4B**) is important for efficient collection of the arrays from the relevant area (**Figure 4C**). Hundreds of sections can be collected on a single wafer sequentially or randomly (**Figure 4D**). Depending on the research question, sample screening and acquisition will require a different strategy, which we arbitrary divided into several scenarios. To illustrate different presented scenarios in a more targeted way, we chose several case studies from the different research project.

Analysis of numerous randomly distributed large structures 1-10 μm range (Figure 4E)

Frequently, ultrastructural data are required to validate a hypothesis that arose from several experimental approaches, comparing a standard and experimentally altered condition. In these cases, several sections are typically randomly collected on grids and screened to localize and image the areas of interest. This tactic is usually less systematic and limited to a small number of analyzed sections. We suggest recording overviews of tens/ hundreds of medium-resolution sections from a given ribbon (Figure 4D). For typical sections of 70 nm, 200 sections will span approximately 14 μm , which will contain numerous cells, either entirely or partially, completed within half an hour. As the first step, the low-resolution overview of the entire ribbon is recorded, and the overview helps to omit the sections that show preparation artefacts (e.g., folds, dirt). After, the acquisition can be performed manually or automatically directly on selected parts of the section, or an entire section, using single or mosaic imaging, followed by stitching (Figure 4E). After, images from the selected area can be acquired using high-resolution parameters. For example, mitochondria, nuclei, and microvilli can benefit from such a statistically improved method (Figure 4Ei-iii).

Analysis of multiple small, sparsely distributed structures 500-1,000 nm range (Supplementary Movie 1)

In this scenario, the ROI cannot be simply identified in a low-magnification overview scan, and high-resolution images are needed. In conventional TEM samples, the tedious zooming in and out of the section is necessary until the required feature is found. Often, imaging several independent locations in multiple samples is more relevant statistically than the generation of a single large volume. In such cases, the complexity of manual acquisition grows exponentially. Though several TEM solutions enable the automatic acquisitions or the screening of multiple grids, the size of the grid and serial sectioning challenges frequently make the approach incompatible for many samples. For similar cases, we generate a complete medium-resolution map of an overall ROI in multiple sections at a resolution sufficient to identify the structures of interest. During this lateral screening step, it is advisable to leap several sections at a time, aiming to hit at least a part of the structure of interest when approached randomly. This will largely depend on the overall dimensions of the structure: e.g., if the overall size of the structure is 500 nm and sections are 50 nm thick, at least nine sequential sections in a row will likely contain a portion of the structure of interest. This way, the skipping of 6-7 sections shall be efficient for finding many different kinds of structures in multiple areas. Automatic acquisition of the resolved mosaic maps of selected sections enables careful screening of these sections after their acquisition. Once such a high-resolution map is acquired, several ROIs can be cropped out or used to define additional local imaging areas on ROIs (Supplementary Movie 1). Golgi, centrioles, junctions, microtubules, different types of vesicles are good examples of the structures that might benefit from this scenario (Supplementary Movie 1).

Analysis of sparsely distributed large ROIs in large samples (Figures 4F-4H)

This scenario involves rare events, which are frequently described as "a needle in a haystack" in which the problem is not in ROI identification but its localization. For many samples correlative approach is not a valid option, yet frequently the ROI has a revealing ultrastructure and, when localized, can be identified with high reliability. For these samples, it is essential to apply multilevel acquisition, starting with the pre-screened samples with tens to hundreds of sections at medium resolution. In the software used here, there are two different strategies for obtaining image sets of multiple sections: Recording the Preview images at a higher resolution or acquiring an Array Tile Set with suitable settings (**Figure 4F**). Different specialized cell types in the *Drosophila* gut are randomly distributed (e.g. stem, enteroendocrine cells), and thin sectioned at random orientation. Yet they can be visually distinguished after screening the images obtained using high-resolution parameters either from single sections or as a collection of serial images (**Figure 4G**). After the alignment, the stacks can be rendered using different software solutions (**Figure 4H**, Supplementary Movie 2).

Scenario 1: Intestinal organoids (Figure 5A)

Organoids are fast-becoming one of the most cutting-edge tools of modern life sciences. This near-physiological 3D stem-cell-derived organ model makes possible an accurate study of a range of in vivo biological processes, including tissue renewal, response to drugs, and regenerative medicine. Recently introduced mini-gut tubes³⁴ open up a new generation of organoid technology, closely resembling in vivo tissue physiology, cell-type composition, and homeostasis, enabling broad perspectives for disease modelling, host-microbe interaction, and drug discovery. However, when ultrastructural characterization is required, the localization of different cell types in such large tissue using random samples can be challenging. Also, in variable "infection" assays, it is crucial to ensure that the analysis reveals different developmental stages that affect the tissue. For such studies, statistically significant coverage of the sample is central, yet hard to achieve using the traditional TEM on-grid approach. AT-scenario 1 is beneficial in such cases: many sequential sections can be generated on a wafer (**Figure 5Aii**) and screened using low-resolution parameters to localize the general areas of interest (**Figure 5Aiii**; arrows). These areas can be targeted for further analysis using advanced acquisition parameters (**Figures 5Aiv** and **Figure 5Av**). When a relevant structure is detected (typically a cluster of 5-10 sections once in every 100-300 sections), it is easy to concentrate on each of the structures of interest and acquire single images manually or use the automation features to acquire image volumes across multiple sections.

Scenario 2: *Drosophila* pupal notum (Figure 5B)

Studying cell division and the mechanisms that control progression through the cell cycle is crucial to understanding both standard and altered processes in multicellular organisms. Information that exists is frequently derived from unicellular systems; however, this solution lacks the critical context of the 3D interactions between the cells in a tissue. A single-cell monolayer of the notum, the developing back of the *Drosophila* larva, is a perfect model for the interaction between the epithelial cells in general and cell division in particular³⁵. It is an established model for molecular and cellular interactions studies using the combination of the data available by fluorescent microscopy and genetic manipulations. Abscission, the last step of cell division, assures the final separation between two dividing cells, and characterizing the structural changes that occur during abscission is essential to our understanding of mitosis. However, mitotic divisions in the notum are not easy to localize on the ultrastructural level: the cells are relatively large, compared to the abscission zone (Figure 5B). The ratio between the overall size of the abscission zone and the surface of the section to cover is large (Figure 5Bi). Even though it is possible to localize the abscission zone using the TEM or SBF-SEM methods³⁶, the task is laborious. With this scenario, the automatic medium-resolution overview images of the leaps of 20-40 sections can be used to localize the dividing cells (Figure 5Bii). When such cells are identified, the sections serve as the anchor for closer examination of the sections in the vicinity, and numerous dividing cells can be found and selected for further analysis. This way, the abscission zone can be located and imaged in its entirety (Figure 5Biii). Depending on the question, single high-resolution images or 3-7 image sequences can be collected to cover the depth of the structure (Figure 5Biv).

Scenario 3: Mouse tanyocyte neurons (Figure 5C)

The mouse provides a well-established model for brain development and is well documented on different levels, including by EM. Even though different automated serial-block-face methods have been used extensively to study brain tissue, there are cases where AT is better adapted to collect the necessary data. The hypothalamus is a well-established neuroscience model, a part of the brain that contains multiple neuronal types and functions. Hypothalamic tanyocytes represent a particular subset of ependymogial cells lining the bottom of the third ventricle, with unusually long processes (up to 300 μm) and large endfeet ($\sim 5 \mu\text{m}$)³⁷. This makes them inconvenient for the analysis by either TEM or FIB methods. The task is further complicated when several independent tanyocytes need to be localized and analyzed. One of the approaches to facilitate this task can be semi-correlative targeting, in which the fluorescence map is obtained from the fluorescently labeled samples before fixing and embedding for EM. The sectioning is performed on the area captured by combining the positional information from the fluorescence sample and the flat embedded plastic replica. After that, the AT scenario 3 can be used: the high-level overview mosaic images are generated to reveal the regions with tanyocyte endfeet clusters. Subsequently, automation features in the software are used to set up the acquisition of sequences of the images from one or several areas in a single image or tiled mode. These images can be analyzed separately, as aligned stacks or rendered after that.

The power of the AT method permits the relatively effortless "upgrade" of data from 2D to 3D: the maps are available from the primary acquisition, and the volumes can be obtained from the selected area and its vicinity. The resulting stack can be aligned and subsequently rendered. It is essential

to determine beforehand which resolution and image quality are needed to find ROIs. Imaging should enable recognizing the ROIs, but not beyond this value because acquisition time scales proportionally to pixel dwell time and the inverse square of pixel size.

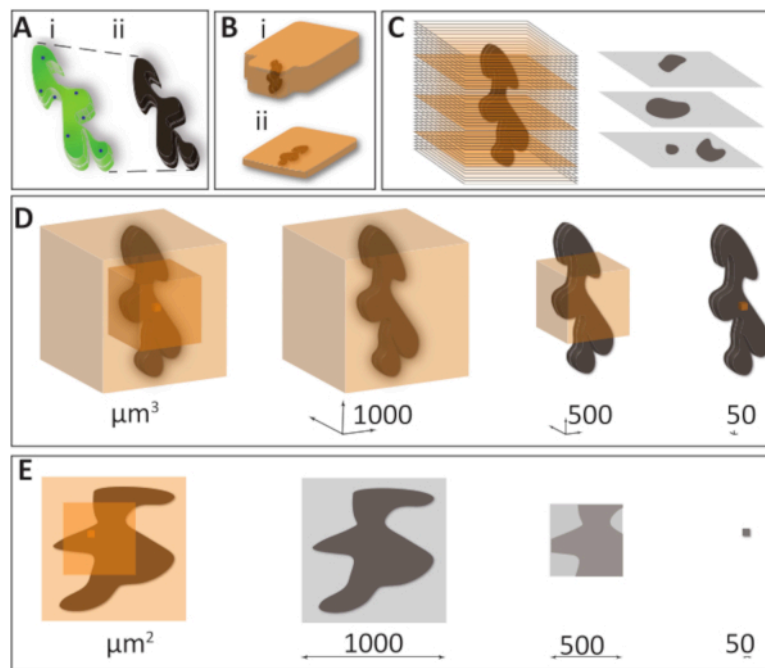


Figure 1: Challenges of EM sample preparation and volume acquisition. (A) The loss of fluorescence and shrinkage happens due to a high heavy metal concentration and dehydration during sample preparation. (i) A schematic drawing of a specimen observed under LM (ii) the same specimen prepared for EM, which becomes completely opaque and loses around 10% of its volume. (B) Sample embedding is typically done using epoxy or acrylic resins. Traditional blocks (i) can be successfully used for homogeneous samples that do not require a particular orientation. Flat blocks (ii) are helpful when it is essential to target and orient under the microscope, a precise area aimed for sectioning, e.g., in non-homogeneous samples or correlative microscopy procedures. (C) Of the entire sample volume, only a limited fraction is represented on a single 50 nm section, providing a 2D image of a 3D sample, frequently in an unfamiliar orientation. (D) To illustrate the problem of recording overly large volumes versus precise targeting, we chose three concentric cubes with the faces of 1000, 500, and 50 μm are organized to include a hypothetical 1000 x 500 x 500 μm sample (dark maroon). If such hypothetical sample cubes are thoroughly sectioned with 50 nm slices, to cover the entire volume, it will require a total of 20,000, 10,000, and 1,000 slices, and 800 tb, 100 tb, and 100 gb, accordingly (imaging resolution 5 nm x 5 nm x 50 nm, 8 bit data). This shows the importance of planning the acquisition of EM data only to acquire the minimum necessary volume. (E) To cover a large sample surface area in high resolution presents a problem similar to that of large volume. Tiling several high-resolution images into one is a helpful solution for such a problem. However, to cover a 1 mm x 1 mm surface using the 2024 x 1048 frame in 10,000x magnification will require a vast number of tiles, which can become challenging to stitch. Further, if sections are variably compressed or distorted during cutting, the resulting data stacks become almost impossible to align. [Please click here to view a larger version of this figure.](#)

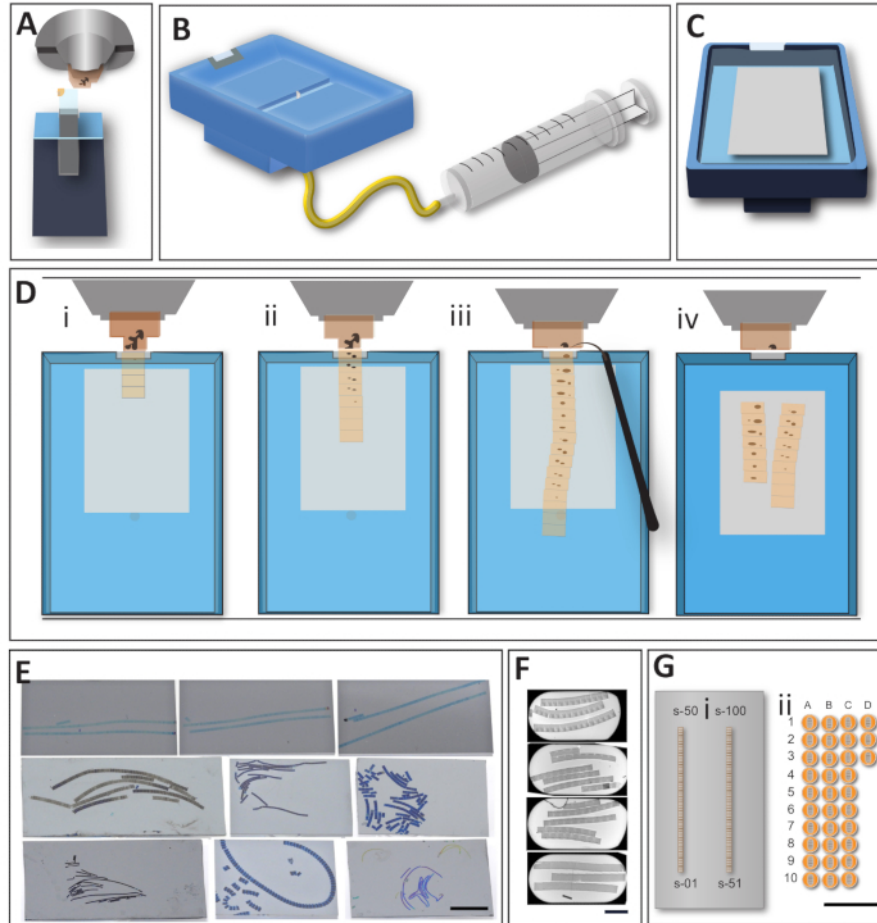


Figure 2: The workflow for the direct generation of the arrays of sections on large support. (A) For tight trimming using the trim tool, blocks are secured inside the microtome holder. This step helps to ensure parallel sides of a block and also reduces empty resin around the sample. (B) A modified knife for AT sections acquisitions. A large boat facilitates the transfer of the sections and their manipulation during sample sectioning and transfer on the support. A large basin enables the manipulation of the sections; the draining system limits the movement of the ribbons during the draining step, the flat bottom makes gradual drying of the support reliable. (C) The knife, ready for sectioning with a glow-discharged wafer placed at the bottom of the basin and water leveled to the edges. The construction of the knife keeps the needle embedded, without interfering with the support. (D) Array generation, top view on the microtome sectioning area. (i) The first sections are usually easy to obtain as they stick to one another and form a regular ribbon. (ii) When more sections are added to the ribbon, and it becomes longer, the ribbon loses its stability and frequently curves. It is crucial to keep the sequence tracks organized in sequence in preparation for the image acquisition step. (iii) When a ribbon of sections reaches the desired length, it is carefully detached from the knife-edge using an eyelash. (iv) Water is drained from the basin; the wafer remains inside until it is entirely air-dry. This step is essential, as it helps to straighten the sections and avoid the formation of the micro folds.

The wafer is placed in the oven at 60°C for at least 30 min to attach the sections on support. **(E)** Example wafers with the transferred sections. Though it is convenient to obtain straight and accurate ribbons, actual samples prevent the formation of such ideal ribbons in most cases. Nevertheless, even "sloppy" ribbons are very informative for the vast number of cases, and the importance of the "neat" ribbon will depend on a research strategy for which the sections are collected. Scale bar 1 cm. **(F)** Example slot grids with the serial sections. Even when many sections are collected on one grid, it is still a tiny fraction of what can be collected on a single wafer. The skill required to master the transfer of the sections on a grid (slot grid in particular) represented a significant bottleneck for mastering electron microscopy sample preparation. Scale bar 500 μm. **(G)** No matter which section collection method was used, the strengths of the AT approach is the relative ease of generation of sequential sections, compared to the on-grid collection. If a 1000 μm x 500 μm sample block is considered, there is no problem to fit around 100 sections on a 2 cm x 4 cm wafer (i). The same size sections on a slot grid will fit only three sections/grid at maximum (ii). We provide a scaled image to show how many grids might be required to cover the same number of sections, not mentioning the difficulty of collecting serial sections on the grid. Scale bar = 1 cm. [Please click here to view a larger version of this figure.](#)

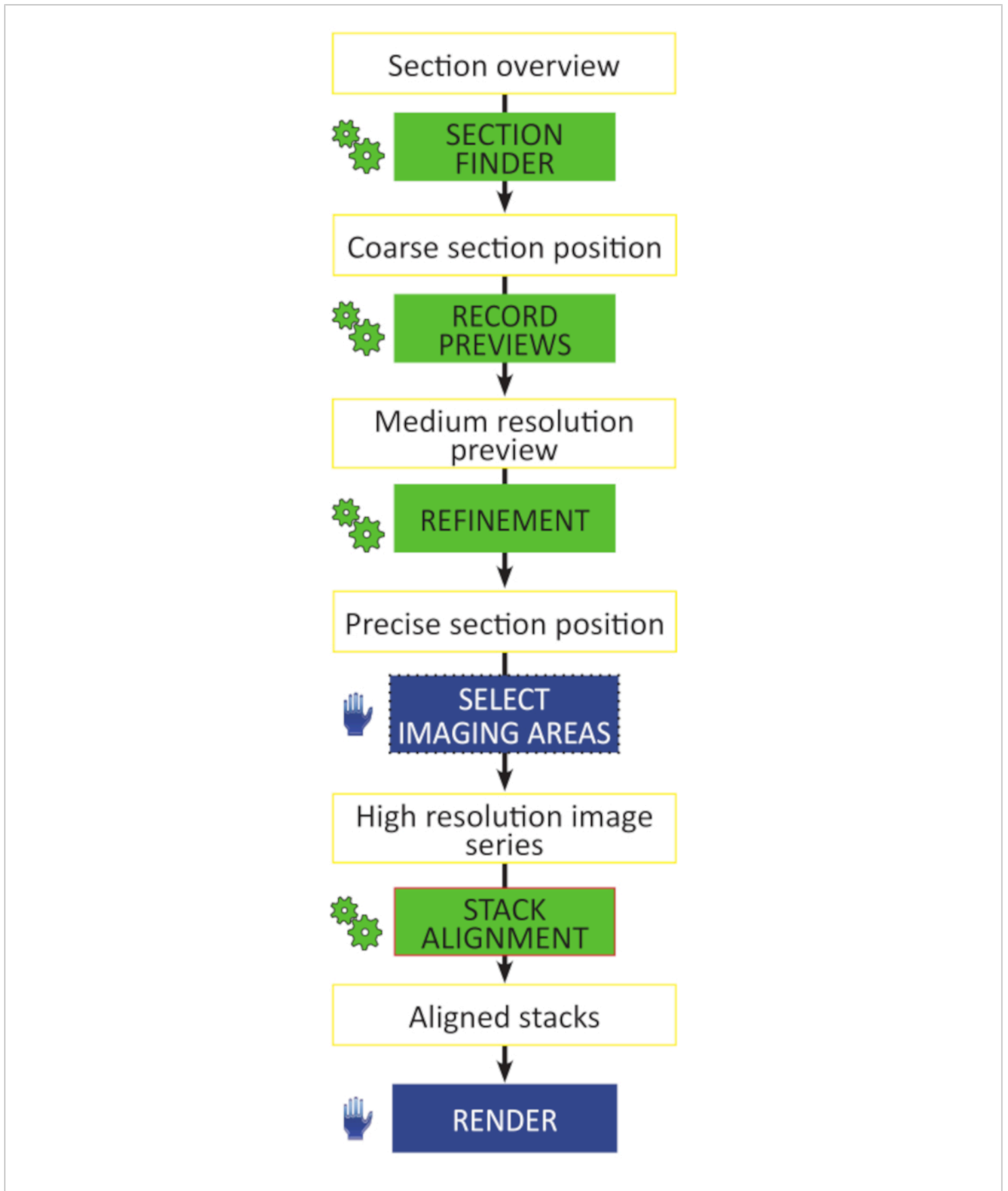


Figure 3: Critical steps of Array Tomography workflow. Schematic of the workflow for the unattended acquisition of high-resolution image stacks. All preparatory steps are automated (green gear symbols) and do not require any actions to be performed manually, section by section. Image stacks can be aligned in any image analysis software capable of automatic rigid or affine alignment. [Please click here to view a larger version of this figure.](#)

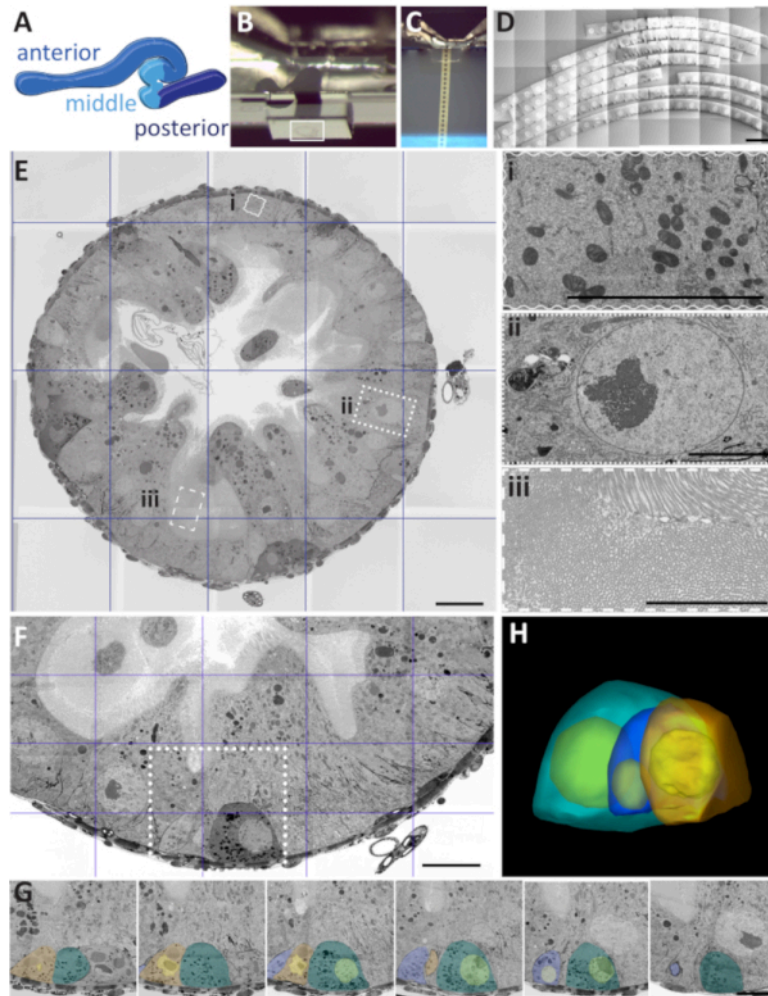


Figure 4: Three acquisition scenarios with *Drosophila* adult gut as a demonstration model. (A) drawing of a dissected *Drosophila* midgut, with three major regions designated by different colors: anterior, middle, and posterior. **(B)** Trimmed flat block in which a gut is oriented for transverse sectioning. Note that the empty resin amount is carefully balanced around the tissue containing the region of interest (white rectangle). **(C)** Transverse serial sections are floating on the water surface inside the basin of the AT knife. All images were acquired in Secondary electron SEM mode using the mirror detector with the inverse contrast. **(D)** Stitched mosaic image of transverse serial sections on a wafer. Scale bar is 1000 μm . **(E)** Cross-section through *Drosophila* gut. Scale bar 20 μm . The image is a stitched mosaic of 7 x 7 mid-range images. Insets - higher magnification and resolution images of the specific regions of interest: (ii) nucleus, (iii) brush border, and (i) mitochondria. Scale bar 5 μm for all. **(F)** A mid-range image of a transverse section through the gut that is targeting the location of developing cells (square). Scale bar is 20 μm . **(G)** The targeted array of serial sections collected based on the area localized during the analysis of the section present in panel F. Scale bar is 10 μm . **(H)** The 3D model is rendered based on the 50

sections stack sequence obtained from the targeted serial acquisition in panel G. [Please click here to view a larger version of this figure.](#)

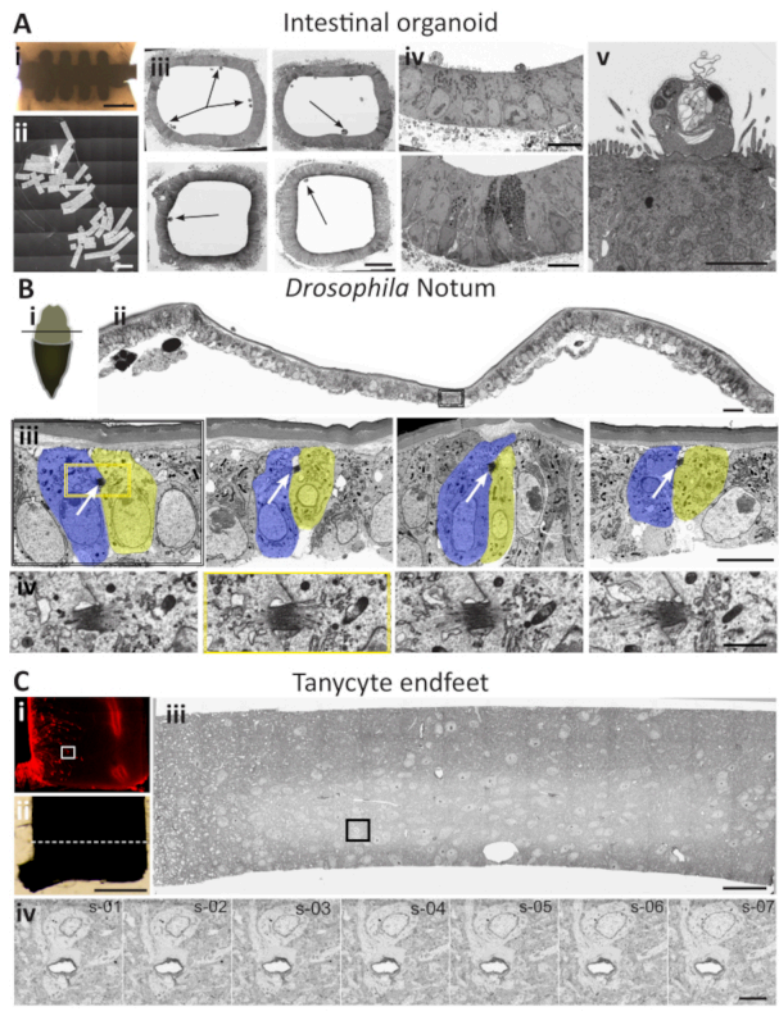


Figure 5: Case studies for the AT application scenarios. (A) Localization of different cell structures in the intestinal organoid. (i) Embedded silicon microchip. Scale bar = 200 μm . (ii) A stitched mosaic image of 127 cross-sections through the central part of the chip. Scale bar = 1500 μm (iii) Four low-resolution images of a complete transverse section through the portion of the intestinal organoid. Arrows point to the potential site of interest. Scale bar is 20 μm . (iv) Different ROIs, targeted on low-resolution micrographs selected for further analysis. Scale bar = 10 μm . (v) High-resolution image of the infected cell of interest. Analysis of the same region in the adjacent sections can provide targeted 3D information if required. Scale bar = 5 μm . **(B)** Midbody localization in *Drosophila melanogaster* pupal notum. (i) A schematic view of a dissected *Drosophila* pupa. Notum exposed for the dissection (beige) after removing the part of the protective cuticle (brown). The black line designates the direction of sectioning (ii) A cross-section through the area presented in the diagram. The image combines 3x7 sequentially taken high-resolution SEM images stitched to one mosaic panel. The black rectangle delimits the area that contains a dividing cell. Scale bar is 15 μm . (iii) A zoomed image on the dividing cell from panel ii. At this magnification and resolution, the midbody is evident (white arrows). The entire section is analyzed to find the dividing cells. Leaping between

different ribbons of sections in 20-30 sections intervals during the lateral screening step permits to localize numerous dividing cell pairs. Scale bar is 5 μm (iv) when a dividing cell is localized, sequential images of the midbody collected from four sections around the midbody delimited by yellow square in the panel (iii). Scale bar is 1 μm . (C) Tanycytes endfeet localization in mouse hypothalamus. (i) Fluorescence image of a vibratome slice. Tanycytes express tdTomato fluorescent protein (red). A white rectangle delimits the area of interest. Scale bar 500 μm . (ii) Same vibratome section prepared for EM will be carefully trimmed around the area of interest-based on the indirect correlation of fluorescent information from panel (i). The dotted white line represents the area of ultrathin sectioning. Scale bar is 50 μm for both panels. (iii) Cross-section through the vibratome slice in the area of interest. SEM mosaic image is composed of 75 stitched images. Several sections are targeted by lateral screening and imaged with similar parameters. The sections are analyzed "offline" in order to find the ROI - the tanycyte endfeet. The black rectangle represents the area that contains the tanycyte endfeet. This section will serve as an anchor for further analysis. Scale bar is 15 μm . (iv) High-resolution, high magnification image of tanycyte endfeet surrounding a blood vessel. After the initial localization of the ROI on one section, the z-sequence is collected from the adjacent sections upstream to the anchor section (panel iii). Scale bar 5 μm . [Please click here to view a larger version of this figure.](#)

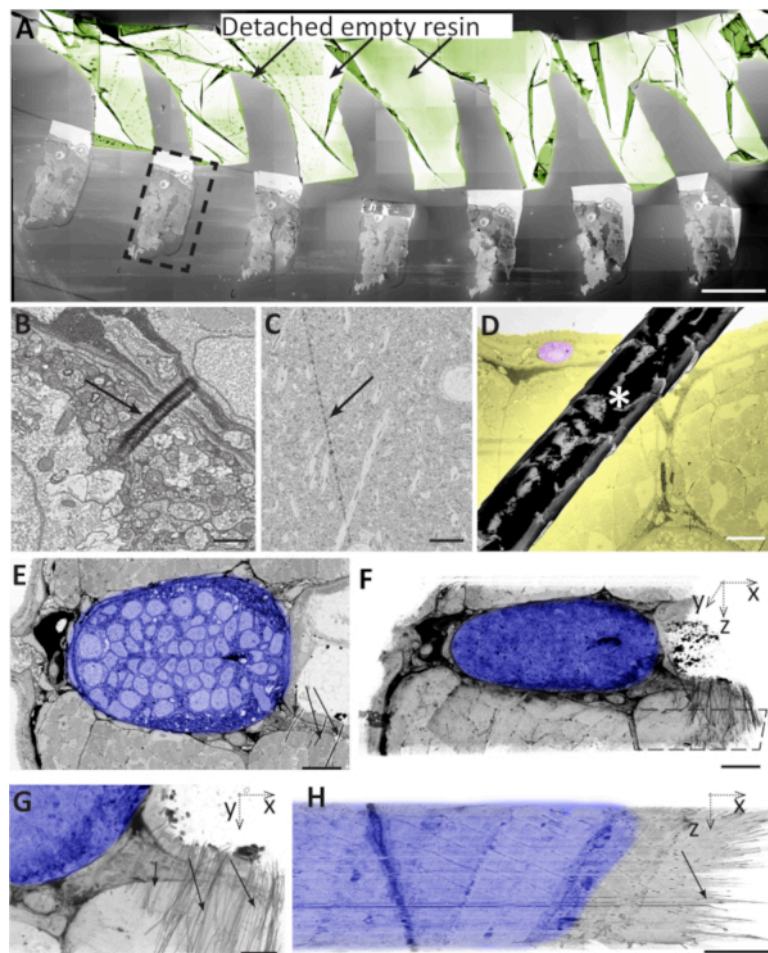


Figure 6: Problems during ultra-microtomy, section collection, and section storage can lead to artefacts. (A) Brain sample sections on a wafer. Most of the empty resin detached from the tissue and folded on itself (sepia). Dashed black box designates an area that is used to contain the entire section. Scale bar 500 μm . (B) A small, local fold on the surface of a 50-nm thick zebrafish section. Scale bar 1 μm . (C) Knife mark on the surface of a 70nm mouse brain section. Scale bar 5 μm . (D) The hair (asterisk) on the surface of the wafer that partially covers a zebrafish muscle section. In yellow, the tissue is targeted for the analysis. In pink, a cell used to serve as a reference for the size of the affected area. Scale bar 50 μm . (E) Zebrafish notochord with wrinkles at the bottom right (black arrows), where dense neural tissue (shadowed in blue) borders on softer muscle tissue and empty resin (black arrows). Scale bar 10 μm . (F) Volume segmentation of a stack of 50 images as in E, showing that this region showed wrinkles in most sections. Dashed polygon outlines the area shown in the G. Scale bar 10 μm . (G) XY view of the same volume segmentation as in F, showing the wrinkles as short black strokes in the right half of the block. Note that the alignment of the stack in the remaining parts of the tissue is not affected by the wrinkles. Scale bar 10 μm . (H) Z-axis view of the same volume segmentation as in F, showing the wrinkles as a vertical line in the right half of the block. Note that the alignment of the stack in the remaining parts of the tissue is not affected by the wrinkles. Scale bar 10 μm .

bar 5 μm . (H) XZ projection of the same area as in G, showing the wrinkles in all 50 sections. Scale bar 5 μm . [Please click here to view a larger version of this figure.](#)

Supplementary movie 1: A high-resolution montage image of a cross-section through *Drosophila* anterior midgut. Mosaic image of an inverted SE-MD SEM image. 352 separate image tiles were automatically acquired at 5 nm resolution and stitched to present the entire cross-section. It is possible to zoom in for more details and get an exhaustive coverage of the data, using the same image. Tight junctions, microtubuli, different types of vesicles can be when zooming in. Scale bar is 10 μm . [Please click here to download this movie.](#)

Supplementary movie 2: *Drosophila* gut cells rendering. Fifty aligned mosaic images of the sections in the area of dividing intestinal cells. IMOD rendering of the cell borders (blue, turquoise, and orange) and nuclei (white). [Please click here to download this movie.](#)

Supplementary Materials. [Please click here to download this file.](#)

Discussion

Electron microscopy gives insight into the ultrastructure of the cells and organisms, for which it is often desirable to image structures of interest in their 3-dimensional context. Despite numerous EM tactics for ultrastructural analysis, there is still no "gold standard" solution. The main reason is the wide variety of samples, many biological questions, which frequently require a tailored approach. The proposed AT workflow is designed to minimize the time necessary for sample processing, data acquisition, evaluation, and storage. Furthermore, the modified knife provides a helpful tool to simplify array acquisition. The compact layout of sections on wafers is convenient, both for the observation and

the subsequent storage of the samples. This arrangement enables "Lateral Screening" of samples by horizontally moving from ribbon to ribbon and scanning only one section on each, significantly reducing the time required to localize an ROI. Proposed data acquisition scenarios facilitate the targeting of small and randomly distributed areas. Once found, AT/SEM restricts high-resolution imaging precisely to the volume of interest, whether performed manually or with the help of automatic function. AT for limited volumes can be completed manually, with the operator navigating through the sample and defining imaging regions one by one. The automated module of the software provides a flexible image acquisition strategy for imaging of small areas on large sections. The automation in this software allows recording large high-resolution images on hundreds of sections, achieving similar volumes as SBFI. Recording overview images of all sections simplifies the ROI localization and reduces the time spent at the microscope. Since the sections are not harmed during the recording of overviews and higher resolution Previews, AT/SEM permits reusing the sample to collect further data of other ROIs or at a higher resolution.

Image acquisition time is one of the most important (and most expensive) aspects of 3D EM and should therefore be considered in the experiment design. While it is unsurprising that imaging large areas takes longer than imaging small areas, it is easy to under-estimate the impact: Depending on the imaging parameters selected, the acquisition time on each section can vary from seconds to hours. Critical imaging parameters include the size of the field of view, resolution, and dwell time. Assuming a target resolution of 10nm per pixel and

1 μs dwell time, imaging a field of $20\ \mu\text{m} \times 20\ \mu\text{m}$, $100\ \mu\text{m} \times 100\ \mu\text{m}$, or $500\ \mu\text{m} \times 500\ \mu\text{m}$ takes 4 seconds, 100 seconds, or 2,500 s to record. We can multiply these per-section imaging times by the number of sections to estimate the time required for the complete imaging job. Long per-section imaging times can be acceptable if the number of sections is small or if microscope tool time is of no concern.

However, it is necessary to limit the recording time to an overnight job or a weekend job in most cases. An equally critical aspect of 3D EM that should be considered, is the amount and structure of the resulting image data. Recording the abovementioned imaging fields in 100 sections generates 400 mb, 10 gb, or 250 gb of image data, respectively; the $500\ \mu\text{m} \times 500\ \mu\text{m}$ images pose the additional issue of being larger than 2 gb each. Many of the software programs used for data evaluation cannot open images of this size.

To reduce imaging time, it is important to choose pixel dwell time to meet the signal-to-noise ratio requirements for the subsequent data evaluation (e.g., reconstruction, tracing), and limit the recordings to defined ROIs. The AT extension of the software facilitates image acquisition in small areas in serial sections. The software supports manual and automatic workflows and many semi-automatic variants: imaging areas can be manually positioned and focused on each section, or the user can use the automatic section finder and position alignment features. Depending on the level of automation chosen and supported by the sample type or imaging goals, the time required for setting up image acquisition in hundreds of sections can take an entire workday (done manually) or only a few minutes. In principle, Array Tomography makes it more challenging than other 3D EM methods to acquire small ROIs; imprecise region placement on consecutive sections must be compensated by acquiring larger areas. For

example, if the ROI is $20\ \mu\text{m} \times 20\ \mu\text{m}$ in size and the section-to-section position variability of imaging fields is $10\ \mu\text{m}$, one needs to acquire $40\ \mu\text{m} \times 40\ \mu\text{m}$ images in order to be sure that the ROI is fully captured in each image, on every section. Real-world image position variability ranges from $100\ \mu\text{m}$ to $<10\ \mu\text{m}$ depending on the availability or quality of software features for position alignment or user's patience. With this software, $10\ \mu\text{m}$ can be achieved without too much manual intervention in most samples.

Like any technique, the AT has several weak points that can influence successful data acquisition, and many are similar to other sectioning-based methods. Lack of homogenous distribution of empty resin versus tissue can result in curved or broken arrays. In extreme cases, sections can detach from the support (**Figure 6A**). Variable compression or stretching during the cutting process can create folds that can disrupt the sample in variable regions on subsequent sections (**Figure 6B**). Knife marks can appear on the surface of the collected sections using a damaged knife (**Figure 6C**). Differences in sectioning conditions can induce occasional section compression and thickness differences. Dust or dirt particles can land on a section and partially obscure the zone of interest (**Figure 6D**). Image acquisition can fail due to imperfect auto-contrast, auto-focus, and auto-stigmator functions. The positioning of automatically created imaging areas can be variable and may fail to capture the ROI in all sections.

Several problems can arise at the stage of stitching and alignment. The automatic stitching of mosaic tiles acquisitions can fail, for example, because of the large empty space inside the sample. Due to a drastic change in shape in 3D, image stacks can be challenging to register. Specially developed programs (e.g., IMOD, Fiji, TrackEM2, MIB, or MAPS-AT)

can facilitate semi-automatic alignment^{32,38,39,40}. More challenging sections can be manually aligned using photo editing software. Unfortunately, some datasets may be impossible to align correctly.

Large samples are challenging for TEM serial sections fitting onto grids; on the other hand, many projects do not justify long automatic acquisition using FIB/SEM or SBF-SEM. The AT is a straightforward alternative to a tedious serial section TEM where collection and manipulation of serial sections on a wafer are more straightforward than with the slot grids. Several strategies were developed to facilitate the collection of the arrays, and we share our method to expand the existing toolkit. In cases where the identification of the ROI is challenging, AT-SEM provides a fundamental advantage, with the efficient screening of the samples where organelle-scale resolution across 50 to 500 sections is required. For larger volumes, the automatic collection AT strategies can be efficiently collected if more sections are required. AT samples can be re-imaged multiple times, facilitating targeted imaging of high-resolution areas based on previously-acquired overview images. We believe that the targeted analysis and reduced oversampling by AT/SEM proposed here decreases the labor and data storage requirements. Ultimately, libraries of sections can be collected and maintained for later reuse and consultation. For volume acquisition, FIB or SBF-SEM approaches offer an excellent solution whenever the ROI is easy to identify on the block face or if large 3D volumes are needed for the analysis. However, FIB/SBF-SEM are less efficient when the high-resolution stack image has to be collected from a defined ROI in a targeted manner. To conclude, the proposed methods for screening of AT samples and the use of medium resolution overview images allow limiting image acquisition to the relevant parts of the section array. Precise aiming of

imaging regions speeds up time-to-data and simplifies data evaluation.

In summary, although the concept of AT/SEM is not novel, its use is still not as widespread as its merits would suggest. Overall, it provides a complementary procedure to other existing EM methods. AT/SEM is compatible with the broadest range of sample preparation protocols and imaging workflows and can be done on any FIB/SEM or SBF-SEM microscope as an accompanying technique. In this paper, we have concentrated on AT for recording ultrastructural data from samples that are less likely to be successfully addressed by other methods. We hope that the described procedure for convenient collection of sections and considerably automated acquisition strategies will aid in the first attempts for those who have never encountered the method and will help to perfect it for those who already have some experience.

Disclosures

The author Tilman Franke is an employee of Thermo Fisher that manufactures electron microscopes and piloting programs that are used in the article.

Acknowledgments

We want to thank the members of the EM facility of the University of Lausanne for their support during this development of different steps of the AT procedure. We would like to thank Gareth Griffiths, Marta Rodrigues, Urska Repnik, Christel Genoud, Helmut Gnaegi, Einat Zelinger, Paola Moreno-Roman, Lucy O'Brien and Lindsay Lewellyn for discussions during the preparation of the manuscript and critical reading. We want to acknowledge the groups that contributed the samples used to demonstrate the different

scenarios: Matthias Lutolf, Michail Nikolaev, Devanjali Dutta, Till Matzat, and Fanny Langlet.

References

1. Luckner, M., Wanner, G. From light microscopy to analytical scanning electron microscopy (SEM) and focused ion beam (FIB)/SEM in biology: Fixed coordinates, flat embedding, absolute references. *Microscopy and Microanalysis*. **24** (5), 526-544 (2018).
2. White, J. G., Southgate, E., Thomson, J. N., Brenner, S. The structure of the nervous system of the nematode *Caenorhabditis elegans*. *Philosophical Transaction of Royal Society of London B Biological Sciences*. **314** (1165), 1-340 (1986).
3. Zheng, Z. et al. A complete electron microscopy volume of the brain of adult *Drosophila melanogaster*. *Cell*. **174** (3), 730-743 (2018).
4. Mulcahy, B. et al. A pipeline for volume electron microscopy of the *Caenorhabditis elegans* nervous system. *Frontiers in Neural Circuits*. **12**, 94 (2018).
5. Schorb, M., Haberbosch, I., Hagen, W. J. H., Schwab, Y., Mastrorade, D. N. Software tools for automated transmission electron microscopy. *Nature Methods*. **16** (6), 471-477 (2019).
6. Baumeister, W., Grimm, R., Walz, J. Electron tomography of molecules and cells. *Trends in Cell Biology*. **9** (2), 81-85 (1999).
7. Hoog, J. L. et al. Organization of interphase microtubules in fission yeast analyzed by electron tomography. *Developmental Cell*. **12** (3), 349-361 (2007).
8. Weber, M. S., Wojtynek, M., Medalia, O. Cellular and structural studies of eukaryotic cells by cryo-electron tomography. *Cells*. **8** (1) 57 (2019).
9. Micheva, K. D., Smith, S. J. Array tomography: a new tool for imaging the molecular architecture and ultrastructure of neural circuits. *Neuron*. **55** (1), 25-36 (2007).
10. Horstmann, H., Korber, C., Satzler, K., Aydin, D., Kuner, T. Serial section scanning electron microscopy (S3EM) on silicon wafers for ultra-structural volume imaging of cells and tissues. *PLoS One*. **7** (4), e35172 (2012).
11. Hayworth, K. J. et al. Imaging ATUM ultrathin section libraries with WaferMapper: a multi-scale approach to EM reconstruction of neural circuits. *Frontiers in Neural Circuits*. **8**, 68 (2014).
12. Kubota, Y. et al. A carbon nanotube tape for serial-section electron microscopy of brain ultrastructure. *Nature Communication*. **9** (1), 437 (2018).
13. Wacker, I. U., Veith, L., Spomer, W., Hofmann, A., Thaler, M., Hillmer, S., Gengenbach, U., Schröder, R. R. Multimodal Hierarchical Imaging of Serial Sections for Finding Specific Cellular Targets within Large Volumes. *Journal of Visualized Experiments*. (133), e57059 (2018).
14. Burel, A. et al. A targeted 3D EM and correlative microscopy method using SEM array tomography. *Development*. **145** (12), (2018).
15. Templier, T. MagC, magnetic collection of ultrathin sections for volumetric correlative light and electron microscopy. *Elife*. **8**, e45696 (2019).
16. Denk, W., Horstmann, H. Serial block-face scanning electron microscopy to reconstruct three-dimensional tissue nanostructure. *PLoS Biology*. **2** (11), e329 (2004).

17. Knott, G., Marchman, H., Wall, D., Lich, B. Serial section scanning electron microscopy of adult brain tissue using focused ion beam milling. *Journal of Neuroscience*. **28** (12), 2959-2964 (2008).
18. Wanner, A. A., Genoud, C., Masudi, T., Siksou, L., Friedrich, R. W. Dense EM-based reconstruction of the interglomerular projectome in the zebrafish olfactory bulb. *Nature Neuroscience*. **19** (6), 816-825 (2016).
19. Smith, D., Starborg, T. Serial block face scanning electron microscopy in cell biology: Applications and technology. *Tissue Cell*. **57**, 111-122 (2019).
20. Kizilyaprak, C., Bittermann, A. G., Daraspe, J., Humbel, B. M. FIB-SEM tomography in biology. *Methods in Molecular Biology*. **1117**, 541-558 (2014).
21. Xu, C. S. et al. Enhanced FIB-SEM systems for large-volume 3D imaging. *Elife*. **6**, e25916 (2017).
22. Hayworth, K. J. et al. Gas cluster ion beam SEM for imaging of large tissue samples with 10 nm isotropic resolution. *Nature Methods*. **17** (1), 68-71 (2020).
23. Maco, B. et al. Correlative in vivo 2 photon and focused ion beam scanning electron microscopy of cortical neurons. *PLoS One*. **8** (2), e57405 (2013).
24. Russell, M. R. et al. 3D correlative light and electron microscopy of cultured cells using serial blockface scanning electron microscopy. *Journal of Cell Science*. **130** (1), 278-291 (2017).
25. Lucas, M. S., Gunthert, M., Gasser, P., Lucas, F., Wepf, R. Bridging microscopes: 3D correlative light and scanning electron microscopy of complex biological structures. *Methods in Cell Biology*. **111**, 325-356 (2012).
26. Koga, D., Kusumi, S., Bochimoto, H., Watanabe, T., Ushiki, T. Correlative light and scanning electron microscopy for observing the three-dimensional ultrastructure of membranous cell organelles in relation to their molecular components. *Journal of Histochemistry and Cytochemistry*. **63** (12), 968-979 (2015).
27. Peddie, C. J. et al. Correlative and integrated light and electron microscopy of in-resin GFP fluorescence, used to localise diacylglycerol in mammalian cells. *Ultramicroscopy*. **143**, 3-14 (2014).
28. Markert, S. M. et al. 3D subcellular localization with superresolution array tomography on ultrathin sections of various species. *Methods in Cell Biology*. **140**, 21-47 (2017).
29. Kolotuev, I., Schwab, Y., Labouesse, M. A precise and rapid mapping protocol for correlative light and electron microscopy of small invertebrate organisms. *Biology of the Cell*. **102** (2), 121-132 (2009).
30. Kolotuev, I. Positional correlative anatomy of invertebrate model organisms increases efficiency of TEM data production. *Microscopy and Microanalysis*. **20** (5), 1392-1403 (2014).
31. Kato, M., Kolotuev, I., Cunha, A., Gharib, S., Sternberg, P.W. Extrasynaptic acetylcholine signaling through a muscarinic receptor regulates cell migration. *Proceedings of the National Academy of Sciences*. **118** (1), e1904338118 (2021).
32. Schindelin, J. et al. Fiji: An open-source platform for biological-image analysis. *Nature Methods*. **9** (7), 676-682 (2012).
33. Miguel-Aliaga, I., Jasper, H., Lemaitre, B. Anatomy and physiology of the digestive tract of *Drosophila melanogaster*. *Genetics*. **210** (2), 357-396 (2018).

34. Nikolaev, M. et al. Homeostatic mini-intestines through scaffold-guided organoid morphogenesis. *Nature*. **585** (7826), 574-578 (2020).
35. Knoblich, J. A. Mechanisms of asymmetric stem cell division. *Cell*. **132** (4), 583-597 (2008).
36. Daniel, E. et al. Coordination of septate junctions assembly and completion of cytokinesis in proliferative epithelial tissues. *Current Biology*. **28** (9), 1380-1391 (2018).
37. Pasquettaz, R. et al. Peculiar protrusions along tanycyte processes face diverse neural and non-neural cell types in the hypothalamic parenchyma. *Journal of Comparative Neurology*. (2020).
38. Kremer, J. R., Mastronarde, D. N., McIntosh, J. R. Computer visualization of three-dimensional image data using IMOD. *Journal of Structural Biology*. **116** (1), 71-76 (1996).
39. Cardona, A. et al. TrakEM2 software for neural circuit reconstruction. *PLoS One*. **7** (6), e38011 (2012).
40. Belevich, I., Joensuu, M., Kumar, D., Vihinen, H., Jokitalo, E. Microscopy image browser: A platform for segmentation and analysis of multidimensional datasets. *PLoS Biology*. **14** (1), e1002340 (2016).